Available online at www.sciencedirect.com
SCIENCE DIRECT
Computational Materials Science 36 (2006) 79–83
COMPUTATIONAL MATERIALS SCIENCE
www.elsevier.com/locate/commatsci

Structural properties and lattice dynamics of $RbMnCl_3$ crystal

A.N. Vtyurin [a], S.V. Goryainov [b], N.G. Zamkova [a,*], V.I. Zinenko [a], A.S. Krylov [a], S.N. Krylova [a]

[a] *Kirensky Institute of Physics, Krasnoyarsk 660036, Russia*
[b] *Joint Institute of Geology, Geophysics and Mineralogy, Novosibirsk 630090, Russia*

Abstract

Energies and lattice dynamics of cubic and hexagonal phases of $RbMnCl_3$ crystal have been calculated non-empirically within a modified Gordon–Kim model. At normal pressure the crystal has been demonstrated to have a six-layer hexagonal structure. Above 1.1 GPa $RbMnCl_3$ is found to transform into the cubic phase. Calculated lattice vibrational frequencies are compared with available experimental data.

PACS: 63.20.Dj; 64.70.Kb; 77.84.Bw; 78.30.Hv

Keywords: $RbMnCl_3$; Perovskite; Soft mode; Lattice dynamics; Gordon–Kim model; Phase transition

1. Introduction

$RbMnCl_3$ crystal belongs to the family of perovskite-like ABX_3 structures. Crystals of this family may form several structural polytypes with different packing of BX_6 octahedra. Most oxide and fluoride ABX_3 compounds including Rb–Mn fluoride crystallize into a cubic perovskite structure (Fig. 1a), while compounds with highly polarizable anions (like Cl, Br) have a hexagonal structure (Fig. 1b). Structural properties and lattice dynamics of cubic perovskites have been well studied in many ways, including ab initio methods. These methods based on Kohn–Sham equations for wave functions are computationally intensive for crystals of more complex hexagonal structures. The Gordon–Kim approach in its traditional form has been used [1] for the lattice vibration spectrum of hexagonal $RbMnCl_3$. These results qualitatively disagree with experimental Raman data [2]. This work is an attempt to improve the Gordon–Kim model taking into account dipole and quadrapole density distortions [3–5], and applying it to calculate the structure and lattice dynamics of $RbMnCl_3$ crystal and to study its stability under hydrostatic pressure.

2. Calculation of total energy

Under normal conditions the structure of $RbMnCl_3$ crystal is hexagonal ($P6_3/mmc$ space group with $Z = 6$, Fig. 1b). Every type of ion in the unit cell has two crystallo–graphically non-equivalent positions, and some ions have free coordinates. Table 1 gives calculated and experimental values of the unit cell parameters and ionic coordinates. Calculated structural parameters agree with experimental values within 5% precision that is typical for this method (see [3–5] for detail). Free parameter values calculated in [1] within the framework of the Gordon–Kim model with spherical ions are also presented there, but in this case the cubic structure is more stable than the hexagonal one and disagrees with the experimental data.

The total energy values, calculated in the generalized Gordon–Kim model and individual contributions to the total energy for the hexagonal and cubic structures are shown in Table 2. Formation of hexagonal structures in

* Corresponding author. Tel.: +7 3912 494507; fax: +7 3912 438923.
E-mail address: zinenko@iph.krasn.ru (V.I. Zinenko).

0927-0256/$ - see front matter © 2005 Published by Elsevier B.V.
doi:10.1016/j.commatsci.2005.08.004

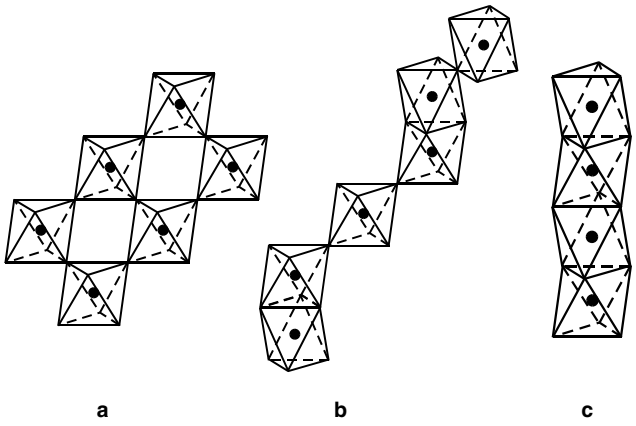

Fig. 1. The arrangement of octahedra in different polytypes of ABX_3: (a) cubic (perovskite) structure, (b) six-layer hexagonal structure, and (c) two-layer hexagonal structure.

Table 2
Calculated values (per molecules) of the total energies and of individual contributions

$E - E^{self}$, eV	Hexagonal phase	Cubic phase, $a = 5.14$ Å
E^c	−33.8317	−34.6722
E^s	2.8239	2.9107
E^c_{d-d}	−0.8318	0.0
E^s_{d-d}	0.1261	0.0
E^c_{q-q}	−0.4500	−0.6357
E^s_{q-q}	0.4072	0.6341
E^c_{d-q}	−0.0850	0.0
E^s_{d-q}	0.0563	0.0
E_{total}	−31.7850	−31.7631

E^c—Madelung energy, E^s—energy of short-range spherically symmetric ion–ion interactions, $E^c_{d-d}, E^c_{q-q}, E^c_{d-q}$—energies of long-range dipole–dipole, quadrapole–quadrapole and dipole–quadrapole interactions, respectively, $E^s_{d-d}, E^s_{q-q}, E^s_{d-q}$—short-range parts of these interactions, respectively. E^{self}—self-energy of an ion.

the rigid ion model was found to be less favorable in terms of energy: because the Mn^{2+} ions are too close to each other there is a loss in the Madelung energy, while the energy of the short-range interactions for both structures is almost equal. The hexagonal structure is stabilized by the polarization energy associated with the interactions between induced dipole and quadrapole moments of ions placed into non-centrosymmetrical positions in this structure. As seen from Table 2, the competition between the long-range Coulomb interaction of point multipoles and the short-range interaction of extended multipoles is very important for lattice stabilization. It should be noted that the hexagonal structure of $RbMnCl_3$ is stabilized by the quadrapole–quadrapole interactions. In compounds with more polarizable anions, such as Br^- in $RbMnBr_3$, the hexagonal structure is stabilized by the energy of dipole–dipole interactions only [6].

The energies of hexagonal and cubic structures are very close and from Fig. 2 which shows the pressure dependence of the difference between the enthalpies of hexagonal and cubic structures it is apparent that under the hydrostatic pressure the structural phase transition from hexagonal to cubic phase is predictable. The calculated transition pressure 1.1 GPa is in good agreement with experimental value 0.7 GPa [2,7]. During this transition the volume of the unit cell decreases, and the resultant cubic unit cell parameter 5.09 Å likewise agrees well with the experimental value of 5.06 Å [7].

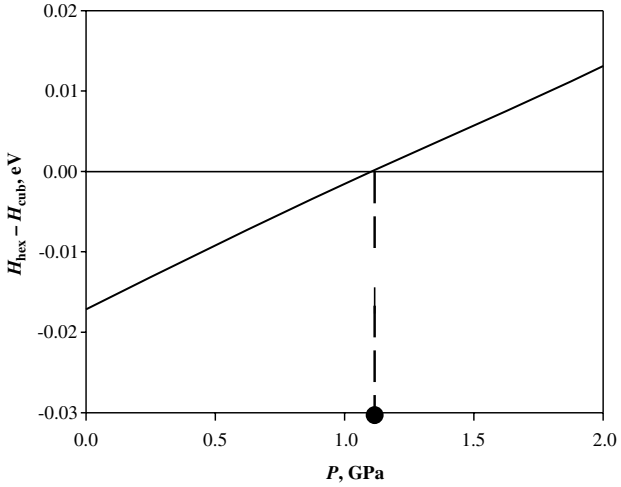

Fig. 2. The pressure dependence of the difference between the enthalpies of hexagonal and cubic structures for $RbMnCl_3$ crystal.

Table 1
Unit cell parameters and coordinates of ions in hexagonal structure

$a = b$, Å				c, Å					
Calc.		Expt. [7]		Calc. [1]			Calc.	Expt. [7]	Calc. [1]
7.09		7.16		7.22			19.04	17.80	18.03
	x/a			y/b			z/c		
	Calc.	Expt. [7]	Calc. [1]	Calc.	Expt. [7]	Calc. [1]	Calc.	Expt. [7]	Calc. [1]
Rb(2b)	0	0	0	0	0	0	1/4	1/4	1/4
Rb(4f)	1/3	1/3	1/3	2/3	2/3	2/3	0.8690	0.9112	0.8920
Mn(2a)	0	0	0	0	0	0	0	0	0
Mn(4f)	1/3	1/3	1/3	2/3	2/3	2/3	0.1543	0.1603	0.1649
Cl(6h)	0.5008	0.4928	0.4925	0.4992	0.5072	0.5230	1/4	1/4	1/4
Cl(12k)	0.1456	0.1616	0.1626	0.8544	0.8384	0.8374	0.1000	0.0820	0.0877

3. Lattice dynamics

The lattice dynamics has been calculated by the generalized Gordon–Kim model also. The expression for the dynamical matrix was given in [5]. The entire phonon spectrum of $RbMnCl_3$ crystal is very complex—90 phonon branches. The acoustic and low-lying optical modes of hexagonal phase spectrum were studied by inelastic neutron scattering in [8], and here we give only a part of the entire phonon spectrum—calculated and experimental (Fig. 3). Table 3 shows calculated and experimental (measured by Raman scattering [2]) phonon frequencies in the Brillouin zone center of the hexagonal phase. For comparison the frequencies calculated within the rigid ion model [1] are also given. Apparently the calculated frequencies are in reasonable agreement with the experimental ones, deviating most in the higher frequency range. Imaginary frequencies of lattice vibrations indicate structural instability of the hexagonal phase. It should be noted that these unstable modes occupy all the phase space of the Brillouin zone. The last column of Table 3 gives the calculated frequencies at the boundary point $A(0,0,\pi/c)$ of the Brillouin zone. The modes at this point are twice and four times degenerated.

The calculated values of optical dielectric constant, elastic constants and Born effective charges are given in Table 4, together with the known experimental data. It is of interest to point out the anomalous large z-components of effective charge tensors (more than twice as large as the nominal ionic charge) of the Mn(2a) and Cl(12k) ions, which form $MnCl_6$ octahedrons. As opposed to that, the effective charges of the Mn(4f) and Cl(6h) belonging to the Mn_2Cl_9 face-bounded double-octahedrons, are significantly closer to their nominal ionic values +2 and −1. It should be noted

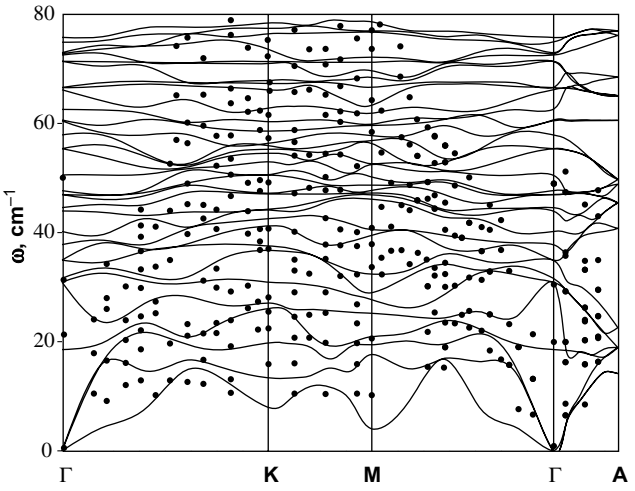

Fig. 3. Calculated acoustic and low-lying optical dispersion curves for hexagonal phase of $RbMnCl_3$ crystal; points—experimental data [8].

Table 3
Vibration frequencies in the hexagonal phase (in cm^{-1})

Zone center $\Gamma(0,0,0)$								Point A $(0,0,\pi/c)$
Ir. Rep.	Present work	Calc. [1]	Expt. [2]	Ir. Rep.	Present work	Calc. [1]	Expt. [2]	
A_{1g}	40	40	55	E_{1g}	11i	44		69i(2)
A_{1g}	89	161		E_{1g}	55	120	55	65i(2)
A_{1g}	111	254	138	E_{1g}	71	157	80?	42i(4)
A_{1g}	136	339	178	E_{1g}	91	171	111	30i(4)
A_{1g}	199	368	260	E_{1g}	148	301	153	18i(4)
A_{1u}	65i	20i		E_{1g}	34i	51i		14(4)
A_{2g}	61	63		E_{1u}	40i	40		19(4)
A_{2g}	70i	71		E_{1u}	0	0		23(2)
A_{2u}	0	0		E_{1u}	19	56		41(2)
A_{2u}	38	35		E_{1u}	48	64		45(4)
A_{2u}	63	56		E_{1u}	73	119		49(2)
A_{2u}	73	146		E_{1u}	79	171		50(4)
A_{2u}	89	202		E_{1u}	102	242		61(2)
A_{2u}	144	271		E_{1u}	125	244		65(4)
A_{2u}	185	352		E_{1u}	157	330		68(2)
B_{1g}	32	26		E_{2g}	16i	39		76(2)
B_{1g}	66	62		E_{2g}	35	55	49	77(4)
B_{1g}	73	99		E_{2g}	47	80	60	85(2)
B_{1g}	80	174		E_{2g}	76	143	78	87(4)
B_{1g}	143	296		E_{2g}	96	216	154	91(4)
B_{1g}	198	356		E_{2g}	103	242	174	102(4)
B_{1u}	60	74		E_{2g}	149	306	218	108(2)
B_{1u}	69i	44i		E_{2g}	26i	39i		122(4)
B_{2g}	65i	53i		E_{2u}	8i	7		129(2)
B_{2u}	44	53		E_{2u}	43i	42		141(2)
B_{2u}	58	112		E_{2u}	31	82		148(2)
B_{2u}	106	221		E_{2u}	67	135		149(4)
B_{2u}	126	276		E_{2u}	89	166		157(4)
B_{2u}	151	339		E_{2u}	118	215		199(2)
B_{2u}	216	391		E_{2u}	157	328		216(2)

Table 4
Calculated values of dielectric constant ε_∞, elastic constants $C_{\alpha\beta}$ (in kbar) and Born effective charges Z_{ij}

	Hexagonal			Cubic, $a = 5.09$ Å	
	Calc.	Expt.		Calc.	
$\varepsilon_\infty^{xx} = \varepsilon_\infty^{yy}$	3.24			3.37	
ε_∞^{zz}	2.8	2.9 [11]		3.37	
C_{11}	268	450 [12]		384	
C_{12}	92			69	
C_{13}	106	180 [12]		69	
C_{33}	290	500 [12]		384	
C_{44}	100	50 [12]		63	
C_{66}	85	140 [12]		63	
	Z_{xx}	Z_{yy}	Z_{zz}	$Z_{xx} = Z_{yy}$	Z_{zz}
Rb(2b)	1.19	1.19	1.27	1.30	1.30
Rb(4f)	1.27	1.27	1.08	2.90	2.90
Mn(2a)	1.64	1.64	4.85	−0.84	−2.52
Mn(4f)	2.98	2.98	1.99		
Cl(6h)	−0.82	−1.59	−1.33		
Cl(12k)	−0.87	−0.87	−2.19		

that in the two-layer hexagonal structure (Fig. 1c), which contains face-bounded octahedra only and has no motive of the perovskite structure, the effective charges of all ions are closer to their nominal ionic values. This confirms partly the idea [3,9] that these anomalous large dynamical charges of ions in the perovskite structure are rather the result of structure specifics than of electronic structures of the ions that form the crystal [10].

As noted above, the structural phase transition from hexagonal to cubic phase under hydrostatic pressure was observed in the $RbMnCl_3$ crystal. The Raman scattering spectra of $RbMnCl_3$ are measured at room temperature under hydrostatic pressure. Because of the small sample size and strong diffuse scattering, only the higher frequency part of the spectrum was recorded. Transformation of the high-requency part of the spectrum under pressure is shown in Fig. 4. At the center of the Brillouin zone the vibrational representation for the hexagonal phase can be decomposed as

$$\Gamma = 5A_{1g} + 6E_{1g} + 8E_{2g} + A_{1u} + 7A_{2u} + 2B_{1u} + 6B_{2u} + 9E_{1u} + 7E_{2u} + 2A_{2g} + 6B_{1g} + B_{2g}, \quad (1)$$

The vibrational modes with A_{1g}, E_{1g} and E_{2g} symmetry are Raman active. One can write a similar expression for the cubic phase

$$\Gamma = 4F_{1u} + F_{2u}. \quad (2)$$

This expression does not have Raman active vibrations. A strong peak at 260 cm^{-1} of A_{1g}-type vibrations and a weak maximum at 218 cm^{-1} of E_{2g}-type, both corresponding mainly to Mn–Cl stretching modes [7] are observed at the pressure just above normal (Fig. 4). As the pressure increases, the spectral intensity drops down gradually, and completely disappears above 0.75 GPa. This phase transition point agrees satisfactorily with the calculated value of 1.1 GPa and the transition pressure of 0.7 GPa

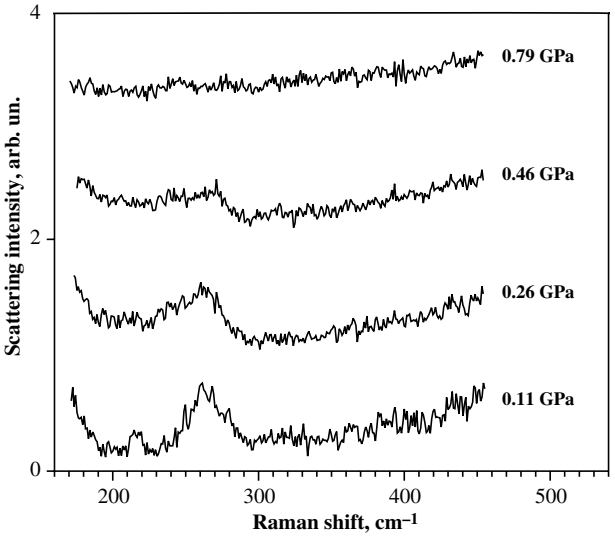

Fig. 4. Pressure-induced transformation of the high-frequency part of $RbMnCl_3$ Raman spectrum.

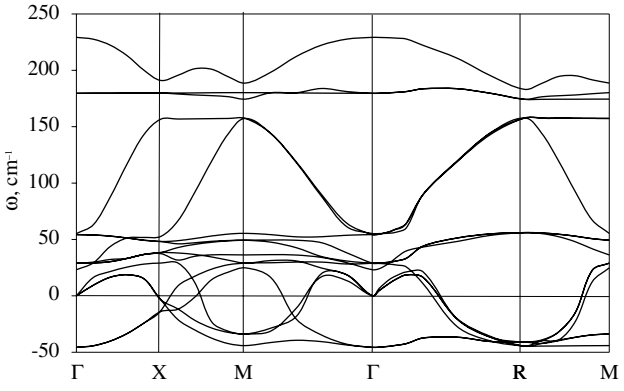

Fig. 5. Calculated dispersion curves for $RbMnCl_3$ crystal in the cubic phase.

reported in [7]. Above this transition point the crystal structure turns into a classic cubic perovskite, and its simulated dispersion curves are given in Fig. 5. This spectrum includes soft phonon branches over whole Brillouin zone including double degenerated soft mode of ferroelectric nature in the Γ–X direction.

4. Conclusion

Thus, our study has found the non-empirical method [3–5] to provide a tool to efficiently simulate the lattice stability and dynamics of ionic crystals with fairly complex structure. In particular, stability of hexagonal phase is predicted for $RbMnCl_3$ crystal and its main parameters (cell parameters, ionic coordinates, elastic and dielectric constants, frequencies of Raman and neutron scattering lines, etc.) are found to be in a reasonably good agreement with experimental data.

The predicted transition from hexagonal to perovskite-like cubic phase has been found by micro-Raman spectros-

copy and experimental transition pressure (0.75 GPa) agrees well with the estimated value (1.1 GPa).

Acknowledgements

This study was supported by Minpromnauki (Grant NSh–939.2003.2) and Russian Academy of Sciences (Project 2.6). One of us (S.V.G.) thanks RFBR (Grant 02-05-65313) and CRDF-BRHE (Grant NO-008-X1) for financial support.

References

[1] M.B. Smirnov, V.Yu. Kazimirov, Krystallography 48 (2003) 480.
[2] A.N. Vtyurin, S.V. Goryainov, N.G. Zamkova, V.I. Zinenko, A.S. Krylov, S.N. Krylova, A.D. Shefer, Phys. Solid State 46 (2004) 1301.
[3] O.V. Ivanov, D.A. Short, E.G. Maksimov, JETP 114 (1997) 333.
[4] O.V. Ivanov, E.G. Maksimov, Phys. Rev. Lett. 69 (1992) 108.
[5] N.G. Zamkova, V.I. Zinenko, O.V. Ivanov, E.G. Maksimov, S.N. Sofronofa, Ferroelectrics 283 (2003) 49.
[6] V.I. Zinenko, N.G. Zamkova, S.N. Sofronova, JETP 96 (2003) 846.
[7] J.M. Longo, J.A. Kafalas, J. Solid State Chem. 3 (1971) 429.
[8] F. Prokert, K.S. Aleksandrov, Kongress und Tagungsberichte der Martin Luther Universitat Halle Wittenberg, Ferroelectrizitat, 1983, p. 51.
[9] O.E. Kvyatkovskii, E.G. Maksimov, Sov. Phys.—Uspekhi 154 (1988) 3.
[10] W. Zhong, R.D. King-Smith, D. Vanderbilt, Phys. Rev. Lett. 72 (1994) 3618.
[11] S.V. Melnikova, A.T. Anistratov, B.V. Beznosikov, Sov. Phys.—Solid State 19 (1977) 2161 (in Russian).
[12] K.S. Aleksandrov, A.T. Anistratov, B.V. Beznosikov, N.V. Fedoseeva, Phase Transitions in Crystals of ABX_3 Halides, Nauka Publishers, Novosibirsk, 1981 (in Russian).